SAIC-01/8020:APPAT-287
November 26, 2001

"GLOBAL MAGNETOHYDRODYNAMIC MODELING OF THE SOLAR CORONA"

NASW-98030

Final Report,

Sept. 30, 1998 - Sept 29, 2001

NASA CONTRACT: NASW-98030

PRINCIPAL INVESTIGATOR:

JON A. LINKER

SCIENCE APPLICATIONS INTERNATIONAL CORPORATION

10260 CAMPUS POINT DRIVE

SAN DIEGO, CA 92121-1578

GLOBAL MAGNETOHYDRODYNAMIC MODELING OF THE SOLAR CORONA

FINAL REPORT:

9/30/98 - 9/29/01

1. Introduction

The solar corona, the hot, tenuous outer atmosphere of the Sun, exhibits many fascinating phenomena on a wide range of scales. One of the ways that the Sun can affect us here at Earth is through the large-scale structure of the corona and the dynamical phenomena associated it, as it is the corona that extends outward as the solar wind and encounters the Earth's magnetosphere. The goal of our research sponsored by NASA's Supporting Research and Technology Program in Solar Physics is to develop increasingly realistic models of the large-scale solar corona, so that we can understand the underlying properties of the coronal magnetic field that lead to the observed structure and evolution of the corona. In the following sections we describe the work performed under this contract.

2. Computational Modeling of the Corona and Inner Heliosphere

Support from this contract has allowed us to develop sophisticated magnetohydrodynamic (MHD) computations of the solar corona and inner heliosphere. A key aspect of the computations are that observed photospheric magnetic fields are incorporated into the boundary conditions, allowing the performance of computations that can be compared with specific observations. To compute self-consistent three-dimensional MHD solutions for the large-scale corona, we solve the following equations in spherical coordinates:

$$\nabla \times \mathbf{B} = \frac{4\pi}{c}\,\mathbf{J} \ , \tag{1}$$

$$\nabla \times \mathbf{E} = -\frac{1}{c}\frac{\partial \mathbf{B}}{\partial t} \ , \tag{2}$$

$$\mathbf{E} + \frac{1}{c}\,\mathbf{v} \times \mathbf{B} = \eta\,\mathbf{J} \ , \tag{3}$$

$$\frac{\partial \rho}{\partial t} + \nabla\cdot(\rho \mathbf{v}) = 0 \ , \tag{4}$$

$$\rho\left(\frac{\partial \mathbf{v}}{\partial t} + \mathbf{v}\cdot\nabla\mathbf{v}\right) = \frac{1}{c}\,\mathbf{J}\times\mathbf{B} - \nabla p - \nabla p_w + \rho\mathbf{g} + \nabla\cdot(\nu\rho\nabla\mathbf{v}) \ , \tag{5}$$

$$\frac{\partial p}{\partial t} + \nabla\cdot(p\mathbf{v}) = (\gamma - 1)(- p\nabla\cdot\mathbf{v} + S) \ , \tag{6}$$

$$S = -\nabla\cdot\mathbf{q} - n_e n_p Q(T) + H_{\rm ch} + H_{\rm d} + D \ , \tag{7}$$

where **B** is the magnetic field, **J** is the current density, **E** is the electric field, ρ, **v**, p, and T are the plasma mass density, velocity, pressure, and temperature, and the wave pressure p_w represents the acceleration due to Alfvén waves. The gravitational acceleration is **g**, $\gamma = 5/3$ is the ratio of specific heats, η is the resistivity, ν is the viscosity, $H_{\rm ch}$ is the coronal heating source, D is the Alfvén wave dissipation term, n_e and n_p are the electron and proton density, and $Q(T)$ is the radiation loss function (Rosner *et al.* 1978). The term $H_{\rm d} = \eta J^2 + \nu\nabla\mathbf{v}{:}\nabla\mathbf{v}$ represents heating due to viscous and resistive dissipation. In the collisional regime (below ~ $10R_S$), the heat flux is $\mathbf{q} = -\kappa_{||}\hat{\mathbf{b}}\hat{\mathbf{b}}\cdot\nabla T$, where $\hat{\mathbf{b}}$ is the unit vector along **B**, and $\kappa_{||} = 9 \times 10^{-7}\ T^{5/2}$ is the Spitzer value of the parallel thermal conductivity. In the collisionless regime (beyond ~ $10R_S$), the heat flux is given by $\mathbf{q} = \alpha n_e k T\mathbf{v}$, where α is a parameter (Hollweg 1978). Since it is presently not known in detail what heats the solar corona, the coronal heating source $H_{\rm ch}$ is a parameterized function (see Lionello, Linker, and Mikic, 2001). Our model can also incorporate the acceleration of the solar wind by Alfven waves using a WKB approximation (Hollweg, 1978) as described by Mikic et al. (1999). Note that the simplified polytropic model is obtained by setting $S = 0$ in Eq. (6), $p_w = 0$ in Eq. (5), and $\gamma = 1.05$.

The methods we use to solve equations (1-7), including the boundary conditions, have been described previously (Mikic and Linker 1994, 1996; Linker et al., 1996; Linker and Mikic, 1997; Mikic et al., 1999; Lionello, Mikic, and Linker, 1999). The principal observational input to our MHD model is the measured line-of-sight photospheric magnetic field. Typically, we have used synoptic magnetic field maps, which are generated from daily measurements of the magnetic field on the visible solar disk in the photosphere and are available from a number of observatories (including Wilcox Solar Observatory, Mt. Wilson Solar Observatory, the National Solar Observatory (NSO) at Kitt Peak and the MDI instrument aboard SOHO).

The radial component of the field (B_{r0}) is deduced from the measured line-of-sight component (Wang and Sheeley 1992). In addition to B_{r0} we must specify the density (ρ_{r0}) and temperature (T_{r0}) as boundary conditions at the lower boundary. A potential magnetic field consistent with the specified B_{r0} and a transonic Parker solar wind solution consistent with the specified ρ_{r0} and T_{r0} are used as initial conditions,

and Equations (1–7) are integrated in time until a steady-state is reached. The plasma flow velocity parallel to the magnetic field at the lower boundary is not specified but is obtained using the MHD characteristic equations. Characteristic equations are also used to calculate quantities at the outer boundary (typically placed at $30R_S$), where the flow is supersonic and super-Alfvenic. The solution obtained provides a 3D description of the solar corona, under the assumption that the large-scale coronal magnetic field is not changing significantly for the time period of interest.

3. Comparisons of the Polytropic Model with Coronal and Heliospheric Data

When S is set to zero, equations (1-7) yield polytropic solutions. These solutions have the advantage that relatively simple models can match many of the properties of the corona; however, values of γ close to 1 (γ = 1.05 for the results shown here) are necessary to produce plasma profiles that are similar to coronal observations (Parker, 1963). Using the plasma density from these computations, we have computed the polarization brightness (pB) as would be observed from Earth or from spacecraft and developed simulated eclipse and coronagraph images that can be compared with corresponding measurements. We have performed extensive comparison of the polytropic model with eclipse observations (Mikic and Linker 1996; Linker et al., 1996; Linker and Mikic, 1997; Mikic et al., 1999), and posted predictions and comparisons of coronal structure on our web site (http://haven.saic.com/corona/modeling.html) for the last 5 total solar eclipses. We have also compared our results with Mauna Loa Coronameter images, LASCO images, coronal holes as deduced from EIT images, and NSO Kitt Peak coronal hole maps (Linker et al., 1999ab). Linker et al. (1999b), Gibson et al. (1999), and Breen et al. (1999) also describe comparisons of our MHD model with observations during Whole Sun Month (WSM; August 10 – September 8, 1996) when a wide range of coronal and heliospheric data was available for coordinated study.

The comparisons discussed above were primarily for times near solar minimum. To extend our technique to compute coronal solutions during solar maximum, two difficulties present themselves. The first problem is that the photospheric magnetic field is changing more rapidly, so synoptic magnetic maps may poorly represent the photospheric magnetic field. The second difficulty is that much higher resolution is required in an MHD computation to capture the highly structured, complex features of the solar maximum corona. Figure 1(a) shows

magnetic field lines for an MHD computation for Carrington rotation 1951 (June 24--July 21, 1999). This calculation was performed in preparation for our prediction of coronal structure during the August 11, 1999 solar eclipse, on a 111 × 141 × 128 nonuniform (r,θ,ϕ) mesh. Note the presence of helmet streamers (regions of closed magnetic field) at nearly all latitudes and the complex nature of the photospheric magnetic field (shown on the solar surface). The predicted radial plasma flow velocity is contoured in the plane of the sky for this view in Figure 1(b). We see that the slow flow regions occur at much higher latitudes in comparison to solar minimum (for example, see Plate 2 of Linker et al., 1999b). Figure 2 shows a comparison of simulated pB images with data from the Mauna Loa MKIII coronameter. Despite the difficulties of computing solar maximum solutions, the MHD model appears to have captured many features of the overall structure of the corona during this time period. However, the Mauna Loa images clearly show more fine structure than is present in the MHD computation, and we also found that the comparisons became worse as the difference between the time of the photospheric measurements and the time of the white-light observations increased. Mikic et al. (2000) describes this calculation in more detail, including our comparison with eclipse images.

We have also extended our MHD calculations of the solar corona out into the inner heliosphere. We have found that the most efficient way to accomplish these computations is to split the calculation into a coronal solution (typically 1-30 R_S) and a heliospheric solution (30 R_S to 5 A.U.) Even with the use of implicit methods, we find that the inner solution requires a time step that is prohibitively small for the heliospheric part of the calculation. A more economical approach is to compute a separate heliospheric solution with a much larger time step. As long as the location of the interface between the calculations is beyond the Alfven and sonic points, it is relatively straightforward to use values from the inner coronal solution as the boundary values for the heliospheric calculation (all the MHD characteristics point outward into the heliosphere, so no information propagates back upstream). We use the magnetic field computed from the coronal solution to specify the boundary condition for the outer solution. At the present time, because the velocity from our polytropic solution does not yield the observed contrast between fast and slow solar wind, we prescribe the velocity at 30 R_S using the topology of the magnetic field (fast flow is assumed to originate from deep within coronal holes, while slow wind is assumed to come from the boundaries of coronal holes). This relatively simple

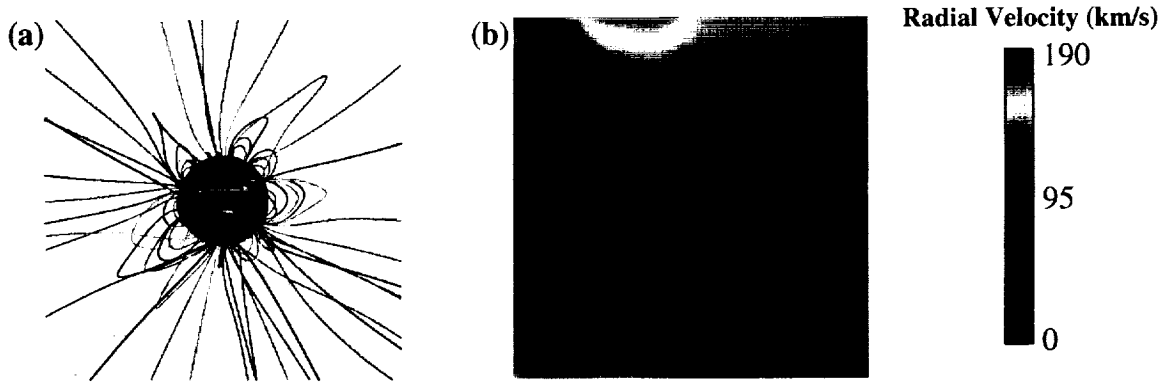

Figure 1. **(a)** Magnetic field lines from a computation of coronal structure near solar maximum (Carrington rotation 1951; June 24 July 21, 1999). Contoured on the solar surface is the photospheric magnetic field deduced from synoptic magnetic field measurements. In contrast to solar minimum, helmet streamers can be seen at nearly all latitudes. **(b)** Color contours of the plasma radial velocity from the model, in the plane of the sky of Figure 1a. Note that the regions of stagnant and slow flow extend to very high latitudes.

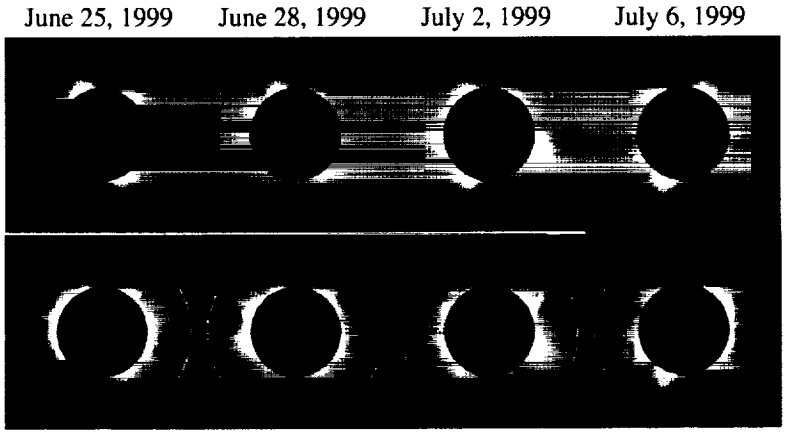

Figure 2. Comparison of results from the MHD model shown in Figure 1 with white light observations. The top panels show the polarization brightness (pB) calculated using the plasma density predicted by the MHD model, and the bottom panels show the observed pB from the Mauna Loa MKIII coronameter. The observed images in general show more structure than is present in the computations, and there are individual discrepancies, but the MHD model appears to have captured the overall structure of the corona. during this interval.

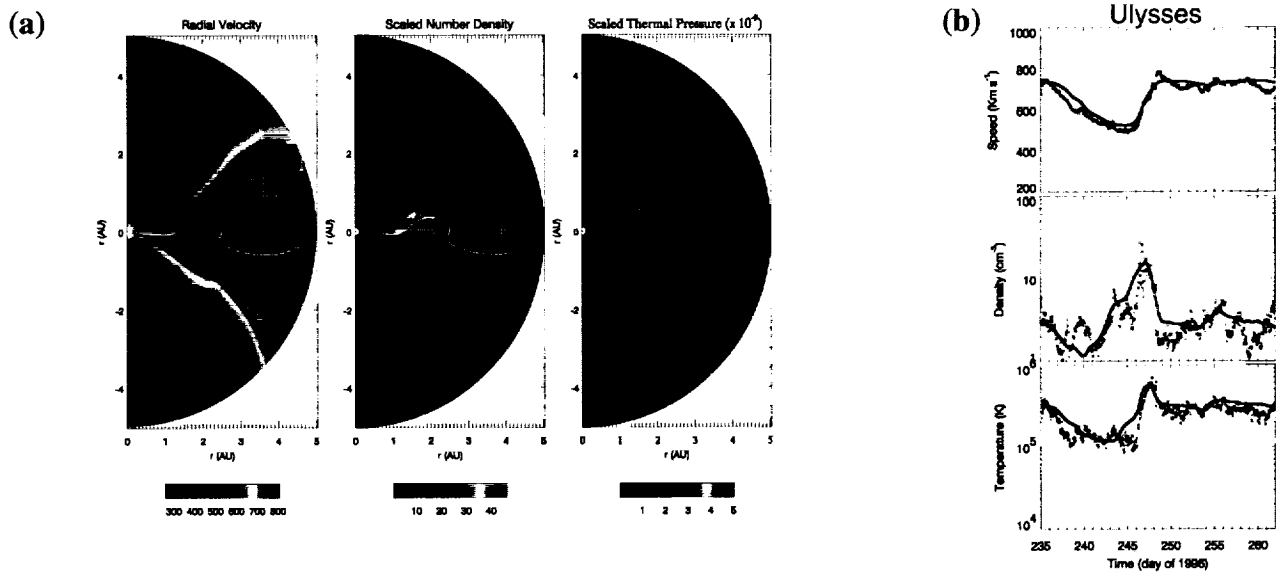

Figure 3. 3D MHD model of the heliosphere during Whole Sun Month (August 10 September 8,1996). (a) Meridional (plane of constant longitude) view of the radial velocity,scaled plasma number density, and scaled plasma pressure. (b) Comparison of Ulysses observations of solar wind speed, proton number density, and proton temperature with the MHD model.

prescription leads to the specification of a complex speed profile at the inner boundary of the heliospheric MHD calculation. (Eventually, the thermodynamic solutions described in section 2.3 will allow us to specify the plasma parameters directly from the MHD solution as well.)

Figure 3(a) shows meridional cuts (planes of longitude) for a calculation of the inner heliosphere performed for the Whole Sun Month time period. Color contours of the radial velocity, scaled plasma number density (to account for the rapid decrease of density with radial distance), and scaled plasma pressure are shown along with the position of the heliospheric current sheet (white line). Note the steepening of the density and pressure that occurs when fast wind catches up with slow wind. During WSM, Ulysses was located at 4.25 AU from the Sun, at a heliographic latitude of 28°N. Figure 3(b) compares Ulysses observations (blue) of bulk flow speed, proton number density, and proton temperature with the simulation results (red), which were obtained by flying the Ulysses trajectory through the model. Overall, the simulation reproduces the large-scale features observed during this time period. Riley et al. (2001ab) describe these and other data comparisons in more detail. Posner et al. (1999,2001) describes additional comparisons of our model interplanetary in situ data, and Breen et al. (1999) discusses comparisons of the model with interplanetary scintillation (IPS) measurements.

We have used our 3D MHD model of the corona and inner heliosphere to explore evolution of the heliosphere over the course of the solar cycle. To illustrate the evolution of the large-scale structure of the HCS during the course of the solar cycle, we present a summary of several solar parameters, measured over a period of ~2-1/2 cycles, together with a selection of simulation results in Figure 4. The central panel includes data from cycles 21, 22, and the ascending phase of 23 and contains: (1) The average computed tilt angle (black) of the HCS as derived from source-surface calculations using photospheric measurements from the Wilcox Solar Observatory by T. Hoeksema (http://quake.stanford.edu/~wso/Tilts.html) and smoothed over 3 Carrington rotations; and (2) Monthly (yearly)-averaged values of Sunspot number in red (blue). Note the significant correlation between the WSO-derived tilt angle and the smoothed sunspot number: Both show a faster rise during the ascending phase of the solar cycle and a slower decay during the descending phase.

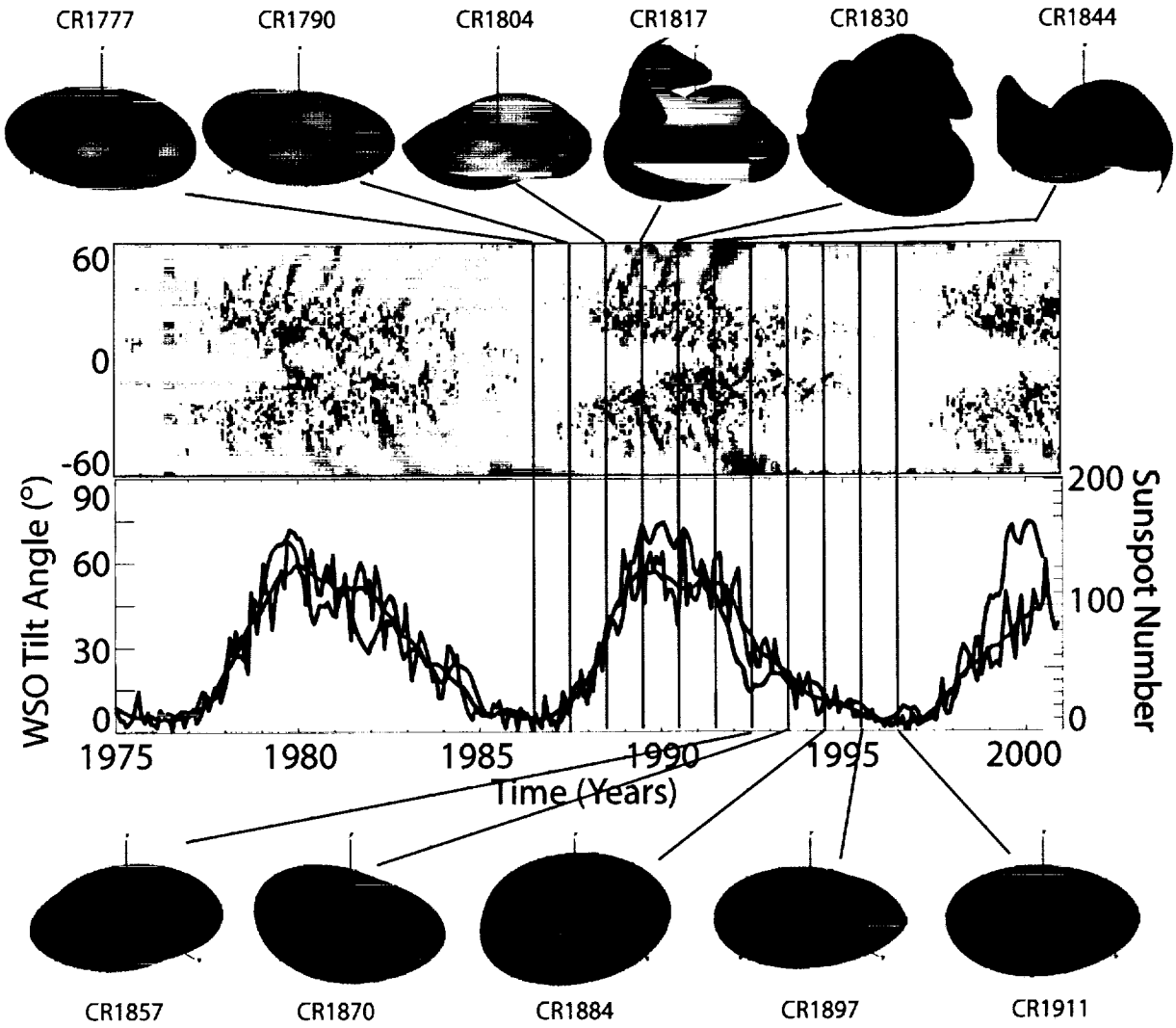

Figure 4. Evolution of several solar parameters during cycles 21, 22, and the ascending phase of 23, with emphasis on the evolution of the HCS during solar cycle 22. The lower-central panel shows the monthly (yearly)-averaged values of Sunspot number in red (blue). The upper-central panel shows the m=0 azimuthally-symmetric part of the radial component of the magnetic field, as inferred from Kitt Peak synoptic maps, for each Carrington rotation. Blue indicates inward polarity and red indicates outward polarity. The HCSs as computed by the MHD model (out to 5 AU) for eleven Carrington rotations, covering mid-1986 to mid-1996, are shown above and below the central panels. Time runs from the top left to right, and then bottom left to right.

The HCS for eleven Carrington rotations, covering mid-1986 to mid-1996, are shown above and below the central panels. Time runs from the top left to right, and then bottom left to right and each simulation is separated from the next by ~13 Carrington rotations. These isosurfaces are in qualitative agreement with the WSO-derived tilt angle profile. In particular, the rapid growth of the HCS to high heliographic latitudes during the ascending phase and the slower decline during the descending phase. A more detailed inspection of the isosurfaces reveals several noteworthy features. First, surrounding solar minimum, the HCS is better described as a flat surface with one or more folds in it, in contrast to the sinusoidal picture that is generated by considering the interplanetary extension of a tilted dipole. Second, folds of the HCS are typically asymmetric with respect to heliocentric distance: A fold rises more sharply on the inner radial side and falls more slowly on the outer radial slide. This is a natural consequence of the dynamic interaction of the surrounding streams and is particularly effective near solar minimum. Adopting a simplified picture of slow solar wind flow being organized about the HCS, and faster flow elsewhere, this asymmetry can be understood by the "stretching" of the HCS on the outer portion of the fold, where a rarefaction region is developing and slower flow is being accelerated into it, and a "squashing" of the HCS on the inner portion of the fold due to the formation of a compression region.

4. Improvements to the Energy Equation

While the results from the polytropic model are encouraging, we know from detailed comparisons that the model is not sophisticated enough to yield the strong temperature variations that are observed in corona. The plasma density from the polytropic model can appear similar to the observations *qualitatively*, but the density contrast between coronal holes and the streamer belt is not accurate *quantitatively*, nor is the solar wind velocity far from the Sun. These difficulties motivated us to formulate a more realistic energy equation (including the terms in S shown in eq. (7)), similar to what had been performed in previous one-dimensional studies (Withbroe, 1988). The inclusion of these energy transport processes into our MHD model allow us to place the lower boundary in the upper chromosphere (T = 20,000 K), and still compute a solution of the large-scale solar corona. We refer to this as our chromospheric MHD model. Figure 5 shows magnetic field lines and the plasma temperature from a two-dimensional

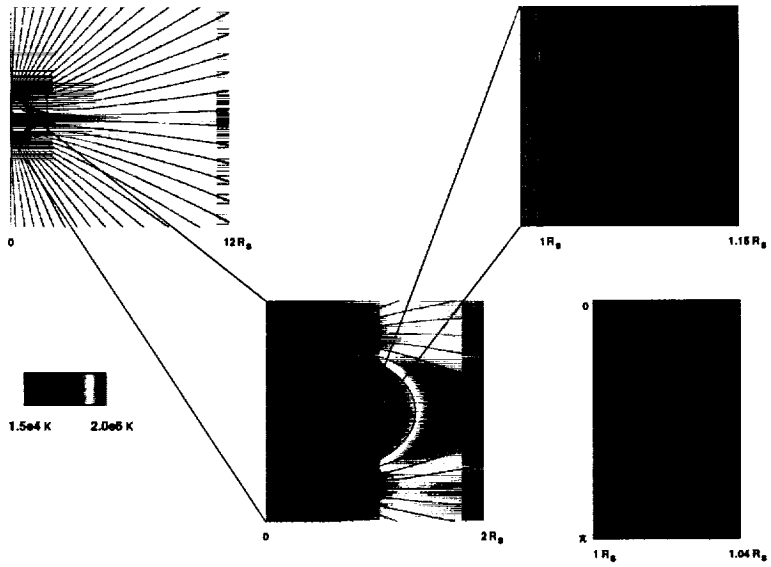

Figure 5. The plasma temperature (T) in the solar corona from an MHD simulation that includes the upper chromosphere and transition region. Also shown are magnetic field lines. Blue shows the lowest temperatures and red the highest. T varies from less than 20,000 K in the upper chromosphere to more than 2,000,000 K in the corona.

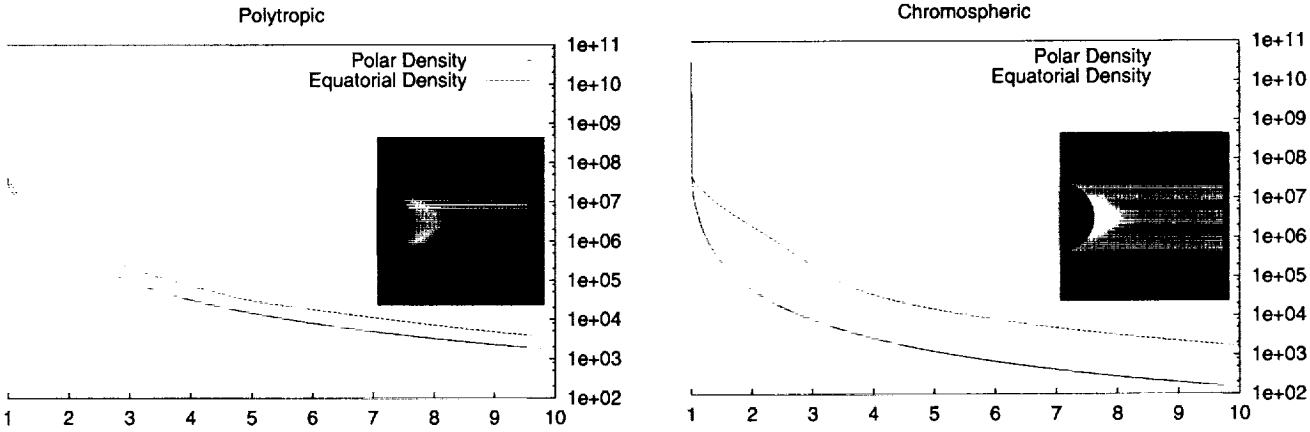

Figure 6. The plasma number density as a function of radial distance for the polytropic and chromospheric MHD models. Note that the chromospheric model incorporates the steep temperature gradient in the lower transition region, and that a much larger contrast between the polar and equatorial density occurs in this model.The inset images show the polarization brighness computed for each model. Note the larger contrast in brightness between the streamer and the polar coronal holes for the chromospheric MHD model.

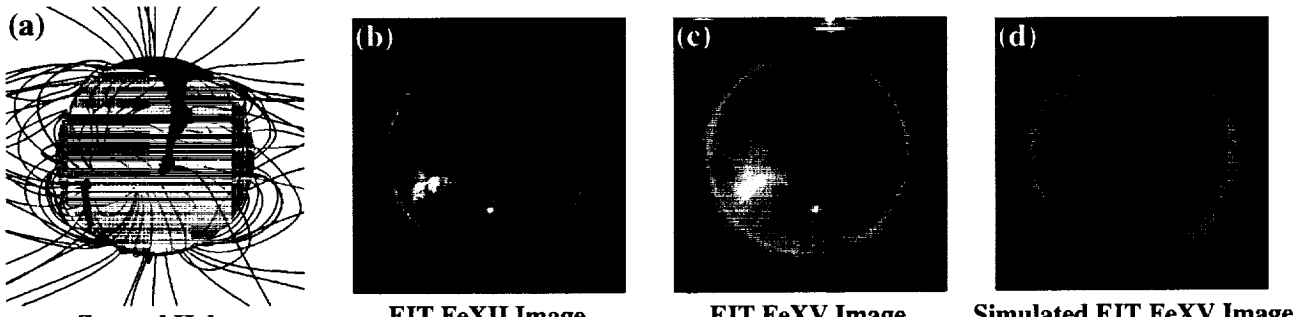

Figure 7. Comparison of EIT images of an equatorial coronal hole on August 27, 1996 with MHD models. **(a)** Open field regions (black) from the polytropic MHD Model.**(b)** EIT 195A image showing the coronal hole. **(c)** EIT 284A image **(d)** Simulated EIT 284A image using the thermodynamic MHD model.

(azimuthally symmetric) calculation as an illustration. The temperature can be seen to vary on a wide range of scales, but is still captured by the model. To capture these sharp density and temperature gradients, the smallest grid cells in our calculation were 70km, or 0.0001 R_S (a nonuniform 200 × 300 r,θ mesh was used). These results are described in more detail by Lionello et al. (2001).

To illustrate the quantitative differences in solutions with the improved model versus the polytropic model, Figure 6 shows radial profiles of the plasma density at the equator and poles for the two different models. In the chromospheric model the equatorial (streamer density) is nearly an order of magnitude greater than the polar (coronal hole density), similar to observations. The polytropic model shows a much weaker density contrast between the equator and pole. The insets show simulated polarization brightness images for these two models. Note that the polar coronal holes are quite dark in the chromospheric MHD model (as is observed). The improved thermodynamic description in our MHD model makes modeling disk emission possible, just as we have previously done for polarization brightness (pB). The more realistic temperature obtained from the solution can be used to predict the abundance of the coronal iron species (using CHIANTI, Dere et al., 1997) and produce ``simulated'' EIT images. To illustrate the idea, we show a comparison we performed for the Whole Sun Month period (Linker et al., 1999b). Open field regions predicted by the polytropic MHD model for August 27, 1996 (Fig. 7a) are compared with EIT images showing an equatorial coronal hole on that day (Fig. 7b and c). For our first 3D computation with our improved thermodynamic model we recalculated the WSM case, and developed a ``simulated'' EIT image (Figure 7d). In this preliminary case we did not include the upper chromosphere, and there is insufficient resolution to reproduce the fine structure seen in EIT, but the model does show low emission in the vicinity of the coronal hole. TRACE emission lines are similar to EIT, and we can use a similar procedure to develop simulated Yohkoh images. In the future, we plan to use simulated emission images to test our models more extensively.

5. Modeling Prominence Formation within a Helmet Streamer

One of our motivations for including the chromosphere is to allow the possibility of realistically modeling prominence formation. As a first step in this type of calculation, we have used a 2.5D axisymmetric MHD model to self-

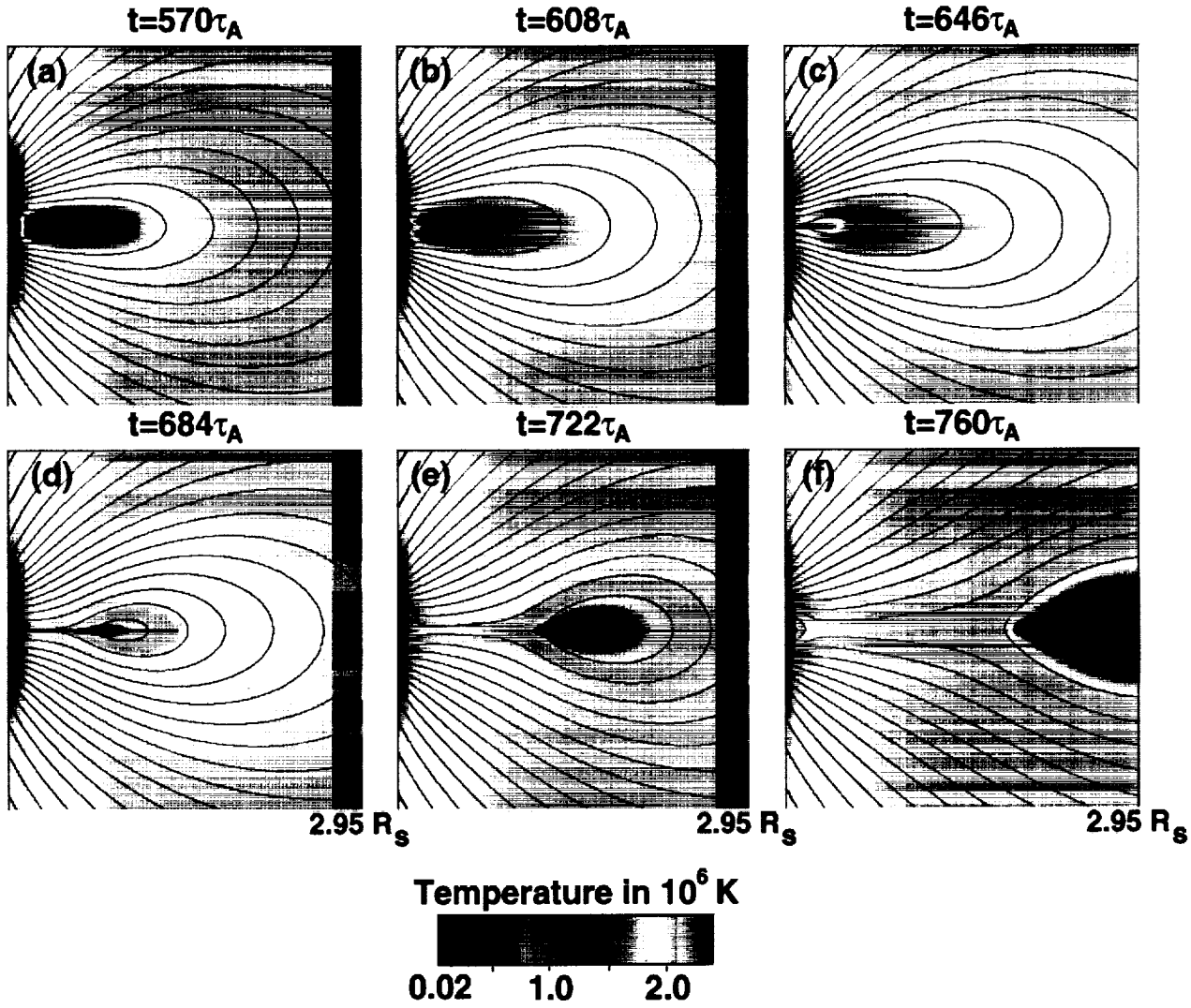

Figure 8. The evolution of the plasma temperature and magnetic field in a thermodynamic MHD model. The plasma temperature is depicted in color, and projections of the magnetic field lines are overlaid on the temperature. A closeup of the lower part of the simulation domain near the equator is shown. **(a)** The helmet streamer configuration at the end of the shearing phase. **(b)** The streamer after the magnetic flux near the neutral line has been reduced 3.75% of its initial value. A low-lying filament structure has formed and is just discernible near the lower boundary. **(c)** The filament is now at a height of 140,000 km and is moving upward slowly. The enhanced density can be seen to lie near the bottom of the detached flux surfaces. Flux reduction (at 11.25%) is beyond the critical threshold for eruption (see text). **(d)** the eruptive phase has started, and dense material is carried into the outer corona, shown in **(e)** and **(f)**.

consistently describe the formation of a stable prominence that supports cool dense material in the lower corona. Reducing the magnetic flux along the neutral line of a sheared coronal arcade creates a magnetic field configuration with a flux-rope topology. Formation of the flux lifts dense chromospheric material into the corona. This prominence-like structure sits at the base of a helmet streamer structure. The dense material is supported against gravity in the dips of the magnetic field lines in the flux rope. Further reduction in magnetic flux leads to an eruption of the prominence, ejecting material into the solar wind. Figure 8 shows the plasma temperature during the formation and ejection of the prominence. A paper describing these results is in press in the Journal of Geophysical Research (Linker et al., 2001).

6. Summary

Support from the NASA SR&T contract "Global Magnetohydrodynamic Modeling of the Solar Corona" has allowed us to greatly advance the state of computational modeling of the solar corona. We have extensively compared our computational models of the corona with eclipse and ground-based coronameter observations (Mikic et al., 1999, 2000; Linker et al., 1999a), observations from the Large Angle Spectroscopic Coronagraph (LASCO) and the Extreme ultraviolet Imaging Telescope (EIT) aboard the Solar and Heliospheric Observatory (Linker et al., 1999b; Gibson et al., 1999) and interplanetary IPS and *in situ* measurements (Breen et al., 1999; Posner et al., 1999, 2001; Riley et al., 2001ab). These comparisons have shown that MHD models can capture many important features of coronal and heliospheric structure, including the location and shape and of the coronal streamer belt, the distribution of coronal holes, the location of fast and slow solar wind streams, and the variation of coronal and heliospheric structure as a function of solar cycle. Inaccuracies of the model in computing coronal temperatures and solar wind velocities motivated us to improve the energy equation in the model and to simulate processes deeper in the solar atmosphere. We have extended the physics in our MHD model to include parallel thermal conduction, coronal heating, and radiation losses in the energy equation (Mikic et al., 1999). These computations can now simulate the top of the chromosphere (at 20,000 K) through the transition region as well as the corona and inner heliosphere (Lionello et al., 2001). We have applied this capability to modeling of prominence formation within a helmet streamer (Linker et al., 2001). A list of our publications follows in the next section.

7. Bibliography

7.1. Publications Partially or Fully Supported by NASW-98030

Amari, T., J. F. Luciani, Z. Mikic, and J. A. Linker, "A twisted flux rope model for coronal mass ejections and two-ribbon flares," *Astrophys. J.*, **529**, L49, (2000).

Breen, A. R., Z. Mikic, J. A. Linker, A. J. Lazarus, B. J. Thompson, P. J. Moran, C. A. Varley, P. J. S. Williams, D. A. Biesecker, and A. Lecinski, "Interplanetary scintillation measurements of the solar wind during Whole Sun Month: Comparisons with coronal and in situ observations," *J. Geophys. Res.*, **104**, 9847, (1999).

Gibson, S. E., D. A. Biesecker, M. Guhathakurta, J. T. Hoeksema, A. J. Lazarus, J. A. Linker, Z. Mikic, Y. U. Pisanko, P. Riley, J. T. Steinberg, L. Strachan, A. Szabo, B. J. Thompson, and X. P. Zhao, " The three-dimensional coronal magnetic field during whole sun month," *Astrophys. J.*, **520**, 871, (1999).

Linker, J., Z. Mikic, D. A. Biesecker, R. J. Forsythe, S. E. Gibson, A. J. Lazarus, A. Lecinski, P. Riley, A. Szabo, and B. J. Thompson, "Magnetohydrodynamic modeling of the solar corona during Whole Sun Month," J. Geophys. Res., **104**, 9809, (1999).

Linker, J. A., Y. M. Wang, E. Marsch, A. Posner, V. Bothmer, and Z. Mikic, " The relationship of fast and slow solar wind to coronal structure," in "Corotating Interaction Regions," (A. Balogh, J. T. Gosling, J. R. Jokipii, R. Kallenbach, and H. Kunow, eds.), Space Science Rev., **89**, p. 146, (1999)

Linker, J. A., R. Lionello, Z. Mikic, and T. Amari, "Magnetohydrodynamic modeling of prominence formation within a helmet streamer," *J. Geophys. Res.*, in press, (2001).

Lionello, R., J. A. Linker, and Z. Mikic, Magnetohydrodynamics of the solar corona and transition region, in *Proceedings of 9th European meeting on Solar Physics*, "Magnetic Fields and Solar Processes," (A. Wilson ed.), p. 1181, ESA Publications Division, Noordwijk, (1999).

Lionello, R., J. A. Linker, and Z. Mikic, "Including the transition region in models of the large-scale solar corona," *Astrophys. J.*, **546**, 542 (2001).

Mikic, Z., J. A. Linker, D. D. Schnack, R. Lionello, and A. Tarditi, "Magnetohydrodynamic modeling of the global solar corona," *Phys. Plasmas*, **6**, 2217, (1999).

Mikic, Z., J. A. Linker, P. Riley, and R. Lionello, "Predicting the Structure of the Solar corona during the 11 August 19999 total solar eclipse," in "The Last Total Solar Eclipse of the Millennium," (W. Livingston and A. Özgüc, eds.), Astronomical Society of the Pacific Conference Series, **205**, 162, (2000).

Posner, A., V. Bothmer, B. J. Thompson, H. Kunow, B. Heber, R. Muller-Mellin, A. J. Lazarus, A. Szabo, J. A. Linker, and Z. Mikic, "In-ecliptic CIR-associated energetic particle events and polar coronal hole structures: SOHO/COSTEP observations for the Whole Sun Month Campaign," *J. Geophys. Res.*, **104**, 9881, (1999).

Posner, A., T. H. Zurbuchen, N. A. Schwadron, L. A. Fisk, G. Gloekler, J. A. Linker, Z. Mikic, and P. Riley, "The origin of open magnetic field-lines at the Sun revealed by composition data and numerical models," *J. Geophys. Res.*, **106**, 15,869 (2001).

Riley, P., J. A. Linker, Z. Mikic, and R. Lionello, "MHD modeling of the solar corona and heliosphere: Comparison with observations," in *Space Weather* (P. Song, G. Siscoe, and H. Singer, eds.), American Geophysical Union, Geophysical Monograph **125**, 159 (2001).

Riley, P., J. A. Linker, and Z. Mikic, "An empirically driven MHD model of the solar corona and inner heliosphere," *J. Geophys. Res.*, **106**, 15,889 (2001).

This contract has also partially or fully supported 7 invited and 24 contributed presentations at scientific meetings.

7.2. References

Breen, A. R., Z. Mikic, J. A. Linker, A. J. Lazarus, B. J. Thompson, P. J. Moran, C. A. Varley, P. J. S. Williams, D. A. Biesecker, and A. Lecinski, *J. Geophys. Res.*, **104**, 9847, (1999).

Dere, K. P., E. Landi, H. E. Mason, B.C. Monsignori Fossi, P. R. Young, and Chianti, *Astron. Astrophys. Suppl. Ser.*, **125**, 149, (1997).

Gibson, S. E., D. A. Biesecker, M. Guhathakurta, J. T. Hoeksema, A. J. Lazarus, J. A. Linker, Z. Mikic, Yu. Pisanko, P. Riley, J. T. Steinberg, L. Strachan, A. Szabo, B. J. Thompson, and X. P. Zhao, *Astrophys. J.*, **520**, 871, (1999).

Hollweg, J.V., *J.Geophys, Res.*, **16**, 689, (1978).

Linker, J. A., R. Lionello, and Z. Mikic, submitted to *J. Geophys. Res.*, (2000).

Linker, J. A., and Z. Mikic, (N. Crooker, J. Joselyn and J. Feynman, eds.), in *Coronal Mass Ejections, Geophys. Monogr.*, **99**, 269, (1997).

Linker, J., Z. Mikic, D. A. Biesecker, R. J. Forsyth, S. E. Gibson, A. J. Lazarus, A. Lecinski, P. Riley, A. Szabo, and B. J. Thompson, *J. Geophys. Res.*, ***104,*** 9809, (1999b).

Linker, J. A., Z. Mikic, and D. D. Schnack, (K. S. Balasubramaniam, S. L. Keil, and R. N. Smartt, eds.) *A.S.P.* **95**, 208, (1996).

Linker, J. A., Y. M. Wang, E. Marsch, A. Posner, V. Bothmer, and Z. Mikic, in "Corotating Interaction Regions," (A. Balogh, J. T. Gosling, J. R. Jokipii, R. Kallenbach, and H. Kunow, eds.), Space Science Rev., **89**, p. 146, (1999a)

Lionello, R., J. A. Linker, and Z. Mikic, *Astrophys. J.*, **546**, 542 (2001).

Lionello, R., Z. Mikic, and J. A. Linker, *J. Comp. Phys.*, **152**, 346, (1999).

Mikic, Z., and J. A. Linker, *Astrophys. J.*, **430**, 898, (1994).

Mikic, Z., and J. A. Linker, in *Solar Wind Eight*, (D Winterhalter, et al., eds.), *AIP Conf. Proceedings*, **382**, 104, (1996).

Mikic, Z., J. A. Linker, P. Riley, and R. Lionello, (W. Livingston and A. Özgüc, eds.), Astronomical Society of the Pacific Conf. Series, **205**, 162, (2000).

Mikic, Z., J. A. Linker, D. D. Schnack, R. Lionello, and A. Tarditi, *Phys. Plasmas, **6***, 2217, (1999).

Parker, E. N., *Interplanetary Dynamical Processes*, Interscience Publishers, New York, (1963).

Posner, A., V. Bothmer, B. J. Thompson, H. Kunow, B. Heber, R. Muller-Mellin, A. J. Lazarus, A. Szabo, J. A. Linker, and Z. Mikic, *J. Geophys. Res.*, **104**, 9881, (1999).

Posner, A., T. H. Zurbuchen, N. A. Schwadron, L. A. Fisk, G. Gloekler, J. A. Linker, Z. Mikic, and P. Riley, *J. Geophys. Res.*, **106**, 15,869 (2001).

Riley, P., J. A. Linker, and Z. Mikic, **106**, 15,889 (2001a).

Riley, P., J. A. Linker, Z. Mikic and R. Lionello, ," in *Space Weather* (P. Song, G. Siscoe, and H. Singer, eds.), American Geophysical Union, Geophysical Monograph **125**, 159 (2001b).

Rosner, R., Tucker, W. H., and Vaiana, G. S. 1978, *Ap. J.*, **220**, 643.Wang, Y. M., and N. R. Sheeley, Jr., *Astrophys. J.*, **392**, 310 (1992).

Withbroe, G. L., *Astrophys. J.*, **325**, 442, (1988).

REPORT DOCUMENTATION PAGE

Form Approved
OMB No. 0704-0188

1. AGENCY USE ONLY (Leave Blank)	2. REPORT DATE	3. REPORT TYPE AND DATES COVERED
	November 26, 2001	3rd Year Annual (Final) Report 9/30/1998–9/29/2001

4. TITLE AND SUBTITLE
Global Magnetohydrodynamic Modeling of the Solar Corona:
3rd Year Annual (Final) Report

5. FUNDING NUMBERS
NASW-98030

6. AUTHORS
Jon Linker

7. PERFORMING ORGANIZATION NAME(S) AND ADDRESS(ES)

Science Applications International Corporation
10260 Campus Point Drive MS A1P
San Diego, CA 92121-1578

8. PERFORMAING ORGANIZATION REPORT NUMBER
SAIC-01/8020:APPAT-287
01-0157-04-1503-000

9. SPONSORING/MONITORING AGENCY NAME(S) AND ADDRESS(ES)

NASA Center for Aerospace Information (CASI)
Parkway Center 7121 Standard Drive
Hanover, MD 21076-1320

10. SPONSORING/MONITORING AGENCY REPORT NUMBER

11. SUPPLEMENTARY NOTES

12a. DISTRIBUTION/AVAILABILITY STATEMENT

NTIS

12b. DISTRIBUTION CODE

NTIS

13. ABSTRACT *(Maximum 200 words)*

In this report we summarize the results from our investigations of the solar corona using magnetohydrodynamic (MHD) simulations.

14. SUBJECT TERMS
Magnetohydrodynamic, solar corona, prominences, CMEs

15. NUMBER OF PAGES
15

16. PRICE CODE
NTIS

17. SECURITY CLASSIFICATION OF REPORT	18. SECURITY CLASSIFICATION OF THIS PAGE	19. SECURITY CLASSIFICATION OF ABSTRACT	20. LIMITATION OF ABSTRACT
UNCLASSIFIED	UNCLASSIFIED	UNCLASSIFIED	UL